

# Measurements dataset of Hydrogen/Air flames in a dual swirl coaxial injector

M. Vilespy, S. Marragou, H. Magnes, A. Aniello, L. Selle, T. Poinso, T. Schuller

March 2023

Version of the database: **HYLON\_TNF\_2023\_04** (April 2023)

Previous version : **HYLON\_TNF\_2023\_01** (January 2023)

When downloading the database, please contact us at [thierry.schuller@imft.fr](mailto:thierry.schuller@imft.fr) to be added to the mail list and be informed of any update.

## 1 Update in the HYLON\_TNF\_2023\_04 version

Previous version of the TNF dataset: HYLON\_TNF\_2023\_01

The update HYLON\_TNF\_2023\_04 includes small changes in the file names and in the pdf file. No changes were made on the available data. The changes made in the HYLON\_TNF\_2023\_04 version are listed below:

- The name of OH\* images folder has been changed to OH\_star to avoid download issues
- In section 5, clarifications about [1] have been added to avoid any misunderstanding when comparing the database and the results presented in [1].

## 2 Abstract

This file provides documentation on the measurements conducted at Institut de Mécanique des Fluides de Toulouse (IMFT) with the HYLON burner, a dual swirl co-axial injector for H<sub>2</sub>/air combustion. Air and H<sub>2</sub> are injected separately into coaxial ducts equipped with swirlers. Two operating points were studied, corresponding to the flames shown in Fig. 1. Flame A is anchored on the hydrogen injector lips. Flame L is lifted above the injector. The experimental setup, operating conditions and measurements of temperature at selected locations in the solid and the flow, velocity field in cold and hot flow conditions, molar fraction of H<sub>2</sub> in cold conditions and NO<sub>x</sub> emissions are described in section 2. Section 3 indicates how the database is organized and how the files are formatted. Publications associated to this database are synthesized in section 4.

## 3 Experimental setup description

### 3.1 HYLON geometry

The experiments were conducted with the HYdrogen LOw NO<sub>x</sub> (HYLON) dual swirl injector shown Fig. 2a [3]. The burner consists of two swirling coaxial ducts to inject fuel and oxidizer separately. The annular channel supplies the air mass flow rate with an external diameter  $d_e = 18$  mm. A swirler made of eight cylindrical vanes of diameter  $d_h = 4$  mm, oriented at 42° with respect to the burner radial direction, is embedded in the external air passage. The inner injector supplies hydrogen through a  $d_i = 6$  mm diameter tube with  $d_{ie} - d_i = 2$  mm lips thickness, which contains an axial swirler of helical shape. According to [3], the external and the internal swirlers generate a flow with swirl number  $S_e = 0.65$  and  $S_i = 0.60$ , respectively. The coaxial burner also features a recess  $z_i = 4$  mm between the hydrogen injector nozzle outlet and the burner backplane that favors mixing of the reactants before burning. The injector feeds a square combustion chamber made of

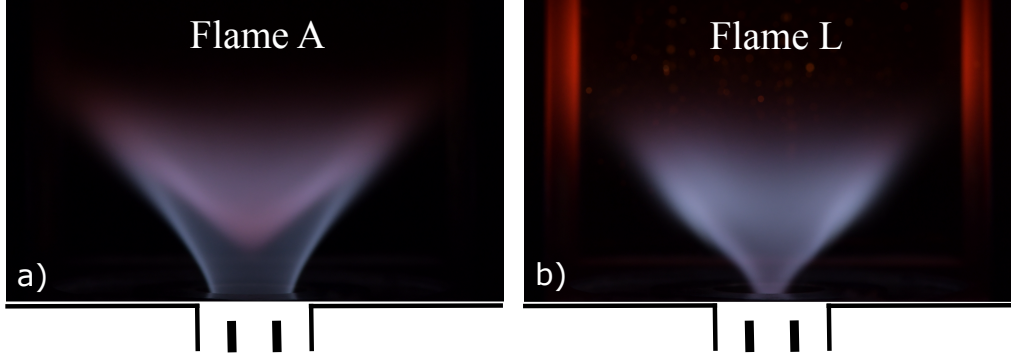


Figure 1: Flame images corresponding to the a) attached flame and b) lifted flame [3, 1].

four fused silica windows to ensure optical access to the flame region, as shown Figs. 2b and 2c. The chamber is  $d_q = 78$  mm wide,  $L_q = 150$  mm long and ends with a 39 mm long nozzle that provides a section reduction to avoid reverse flow at the combustor outlet. The diameter of the exhaust nozzle is  $d_0 = 73$  mm. Details about the injector design can be found in [3, 1].

### 3.2 Operating conditions

Table 1: Operating conditions for flames A and L

Case	$\dot{m}_a$ [g/s]	$\dot{m}_h$ [g/s]	$U_b^a$ [m/s]	$U_b^h$ [m/s]	$T_i^a$ [K]	$T_i^h$ [K]	$P_{th}$ [kW]	$p$ [Pa]	$\Delta p_A$ [Pa]	$\Delta p_H$ [Pa]
A	2.41	0.032	11.4	13.6	298	298	3.89	101325	918	165
L	6.03	0.080	28.5	34.0	298	298	9.73	101325	5752	821

Quantities appearing in Tab. 1 correspond to  $\dot{m}_j$  the mass flow rate in g/s,  $U_b^j$  the bulk velocity in m/s,  $T_i^j$  the temperature in K,  $\Delta p_j$  the pressure drop for air ( $j = a$ ) and hydrogen ( $j = h$ ) injection channels. The thermal power in kW is  $P_{th}$  and  $p$  corresponds the operating pressure in Pa. The global equivalence ratio is kept constant to  $\phi_g = 0.45$ . The operating point A, with a thermal power of  $P_{th} = 3.79$  kW, leads to a flame anchored to the  $H_2$  injector lips. The flame L, with a thermal power of  $P_{th} = 9.73$  kW, is V-shaped and aerodynamically stabilized above the injector [1].

### 3.3 Measurements techniques

All measurements were performed in the axial plane  $y = 0$  mm of the setup shown in Fig. 2b.

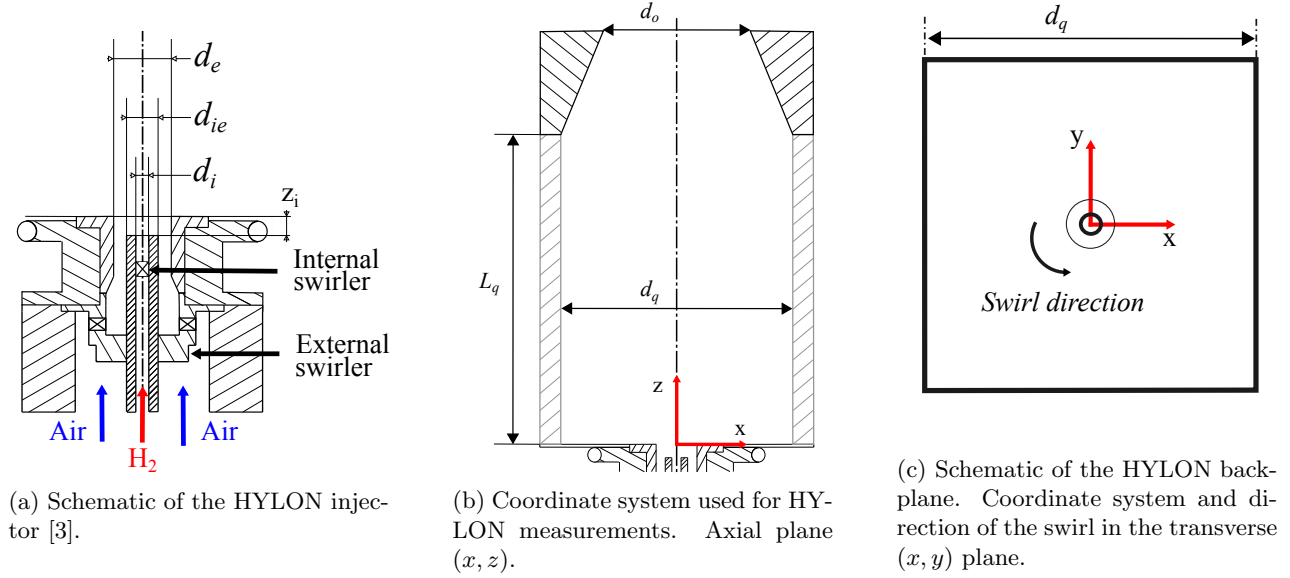


Figure 2: Schematics of the HYLON injector and the combustion chamber.

### 3.3.1 Direct imaging

Direct flame imaging in the visible band is achieved with a Nikon D7500 equipped with a lens Nikkor 105/2.8G AF-S IF-ED VR MICRO. This camera has a wide focal aperture and is used without any color correction. The wide focal aperture allows to take flame images with a small exposure time and with a relatively low intensity which is adapted see lean  $H_2$ /air flames.

### 3.3.2 $OH^*$ imaging

Images of the natural emission of the  $OH^*$  radicals are recorded with an intensified Princeton Instrument PI-MAX4 camera equipped with a UV lens Nikkor Rayfact UV-105 Multispectral lens, 105 mm f/4.5 and a narrow bandpass OD4 optical filter Asahi XHQA310 centered around  $\lambda = 310 \pm 10$  nm. The optical system is described in Fig. 3.

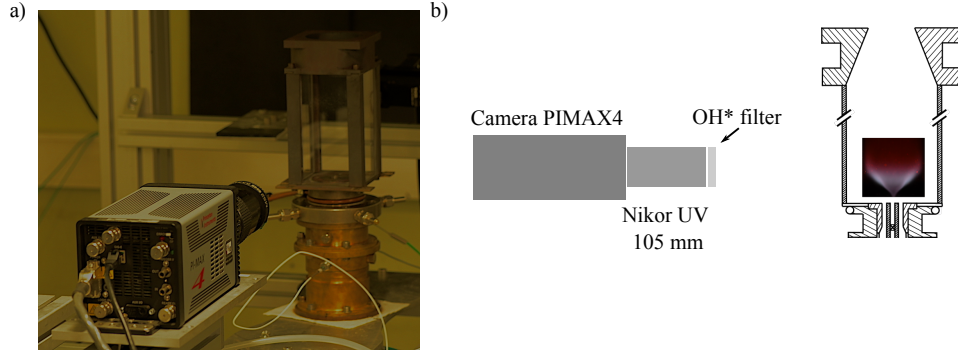


Figure 3: Setup for  $OH^*$  line of sight measurements. (a) Picture of the setup, (b) Schematic of the setup.

### 3.3.3 Pressure drop

The atmospheric pressure outside the chamber is written  $p_0$ . Measurements of the pressure drop  $\Delta p_i$  in each supply channel are made between locations  $p_A$  and  $p_0$  for the air stream  $\Delta p_A = p_A - p_0$  and between locations  $p_H$  and  $p_0$  for the hydrogen stream  $\Delta p_H = p_H - p_0$  using a differential pressure drop sensor SES AUTOMATION SCH-Ex-Cos-P-7500. The position of the probes is shown in Fig. 4.

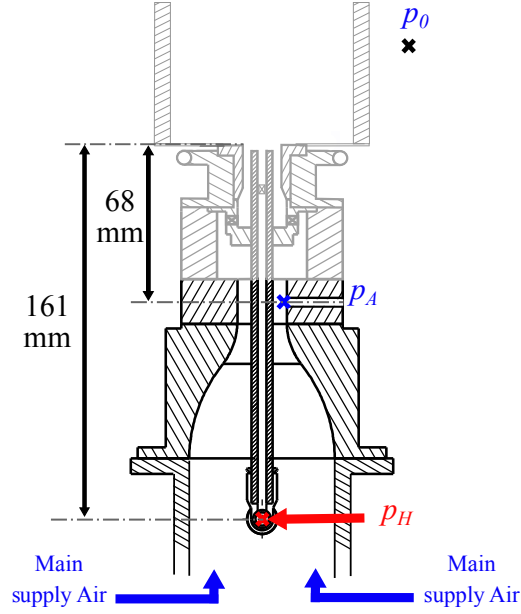


Figure 4: Location of the pressure ports inside the hydrogen channel  $p_H$  and the air channel  $p_A$  for pressure drop measurements.

### 3.3.4 Velocity fields

A PIV system is used in both cold and reactive flow conditions to determine the mean and rms velocity fields in the  $(x, z)$  plane ( $y = 0$ ) of the burner. The system described in Fig. 5 comprises a double-head laser Big Sky CFR200 at 532 nm, a laser sheet generator manufactured by LaVision and a CCD double-shot camera equipped with a bandpass filter  $532 \pm 10$  nm. The camera is a PCO 2000 CCD. The bandpass filter in front of the camera is used to isolate only the scattered laser light by the seeded particles. The particles are alumina oxides ( $\text{Al}_2\text{O}_3$ ) type DX with a diameter equal to  $1 \mu\text{m}$  manufactured by Laborympex.

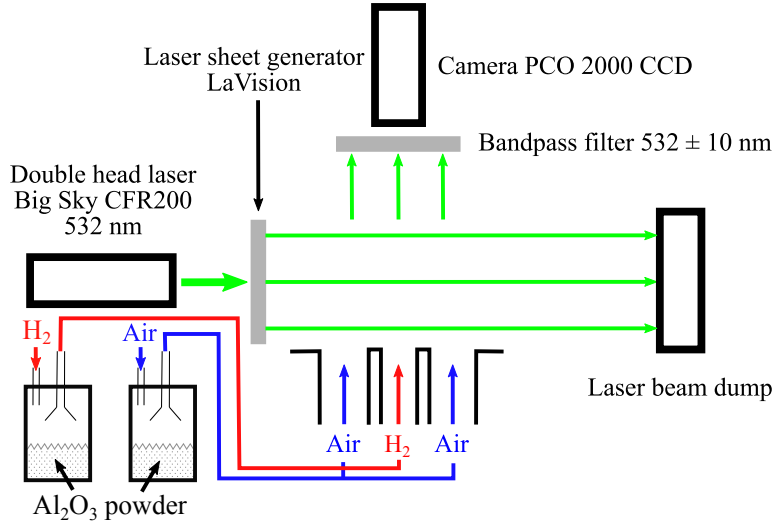


Figure 5: Particle Image Velocimetry optical system used for the 2D velocity field measurements in reactive conditions.

### 3.3.5 Quartz window temperatures

Measurements of the surface temperature on the external side of fused silica windows were made with contact Type-K thermocouples. Thermal paste is applied to improve the quality of the thermal contact between the contact thermocouple and the window. The location of the measurements is described in Fig. 6a.



### 3.3.6 Metallic wall temperatures

Hot surface with temperatures between  $T_s = 250^\circ\text{C}$  to  $T_s = 1200^\circ\text{C}$  were determined with a double wavelength pyrometer Fluke Process Instruments E2RL-F2-V-0-0 Endurance Series. The use of two wavelengths enables to avoid specifying the surface emissivity. A laser pointer eases pointing the measurement locations which are indicated in Fig. 6a-b.

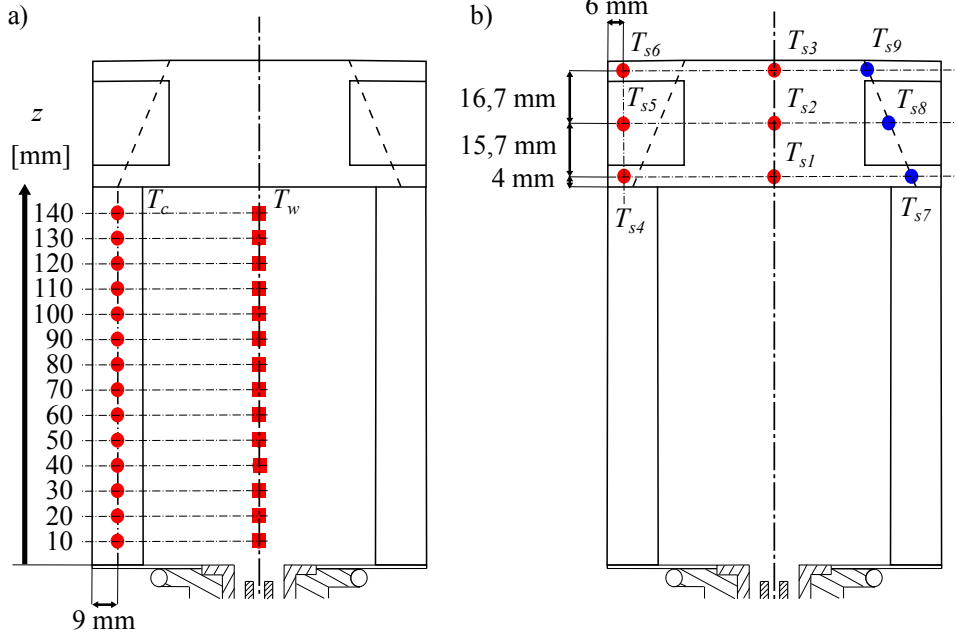


Figure 6: Locations of surface temperature measurements. (a) Measurements along the external surface of the metallic pillar  $T_c$  and along the external side of the fused silica windows  $T_w$ . (b) Measurements at selected locations on the internal and external surfaces of the combustor  $T_s$  [3]. Disk symbols: Measurements with a double wavelength pyrometer. Square symbols: Measurements with the contact thermocouple. Red symbols: External surface of the combustion chamber. Blue symbols: Internal surface of the combustion chamber.

### 3.3.7 Burnt gases temperatures

The measurements of the burnt gases temperature is achieved with two unshielded type-R thermocouples. The first one has a bead diameter  $d_b^1 = 1.80$  mm with wire of  $d_w^1 = 0.80$  mm. The second one has a bead diameter  $d_b^2 = 0.75$  mm with wire of  $d_w^2 = 0.20$  mm. The temperatures measured by the two thermocouples are then post-processed to correct for the impact of thermal radiation using the CRRE method described in [2]. Only the corrected temperature is given in the files. The location of these measurements is indicated in Fig. 7.

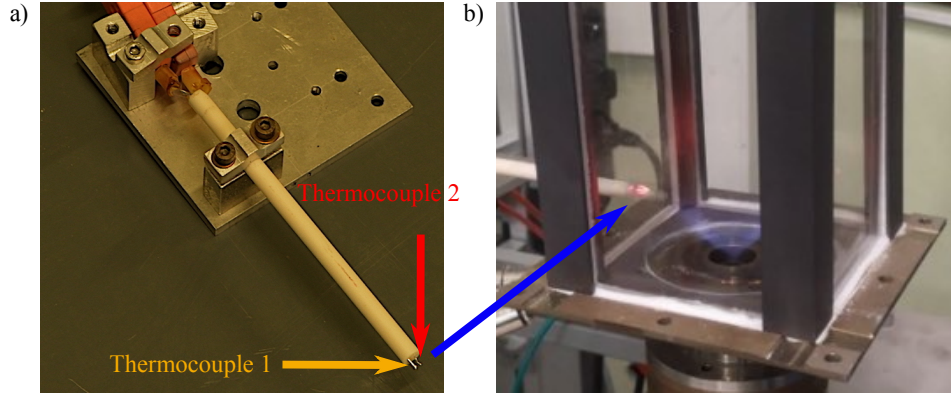


Figure 7: (a) Support with double bead thermocouple used in this work. (b) Double bead thermocouple set in the hot combustion products in the MIRADAS setup [3].

### 3.3.8 NO<sub>x</sub> concentrations in burnt gases

O<sub>2</sub>, NO and NO<sub>2</sub> emissions are measured at the outlet of the combustion chamber using a flue gas analyzer ECOM J2KN enabling measurements in the burnt gases with temperature up to 1100°C. The analyzer is equipped with a dryer to sample dry gases. Characteristics of the sensors are provided in Tab. 2.

Table 2: Sensor principle, range, resolution and accuracy of the measurement for each species analyzed by a ECOM J2KN from the manufacturer.

Measured value	Principle	Range	Resolution	Accuracy
O <sub>2</sub>	EC	0-21 vol. %	0.1 vol. %	±0.3 vol. %
NO	EC	0-500 ppm	0.1 ppm	±5 vol. %
NO <sub>2</sub>	EC	0-100 ppm	0.1 ppm	±5 vol. %

### 3.3.9 Hydrogen concentration profiles

Raman scattering in the cold flow was used to analyze mixing between the air and hydrogen streams with the optical setup described in Fig. 8. It comprises a continuous laser (Coherent Verdi G18) producing a p-polarized laser beam at  $\lambda = 532$  nm. A part of the laser beam is deviated with a beam sampler (Thorlabs BFS10-A) to a power meter (Thorlabs S425C) to monitor the stability of the laser source. The beam is focused in the center of the combustion chamber using a convex-convex spherical lens of 750 mm focal length. In these experiments two fused silica windows are replaced by plates made of aluminium. The focused laser beam passes through a small slit made in the aluminium sidewalls which are painted in black to limit reflection. The luminosity of the laser beam, laser reflections and the Rayleigh scattered light are filtered out by a notch optical filter Edmund Optics 532 ± 15 nm OD4. The remaining scattered light is filtered around 605 nm with an OD4 Edmund Optics 86367 15 nm bandpass filter. This optical system enables to record the light scattered by the N<sub>2</sub> molecules within air by Raman anti-stokes effect around 607 nm. This wavelength corresponds, for an excitation wavelength of 532 nm, to the only vibrational-rotational band of the dinitrogen molecule with a Raman shift equal to 2328.72 cm<sup>-1</sup> [5]. Images of the Raman anti-stokes scattered signal are collected with a PCO Sensicam QE equipped with a Nikkor 105 mm f/2.8G lens. Calibration is made with a set of pure gases before each measurement to deduce the relation between the light intensity and N<sub>2</sub> molar fraction. These data are used to deduce the hydrogen molar fraction  $X_{H_2}$ .

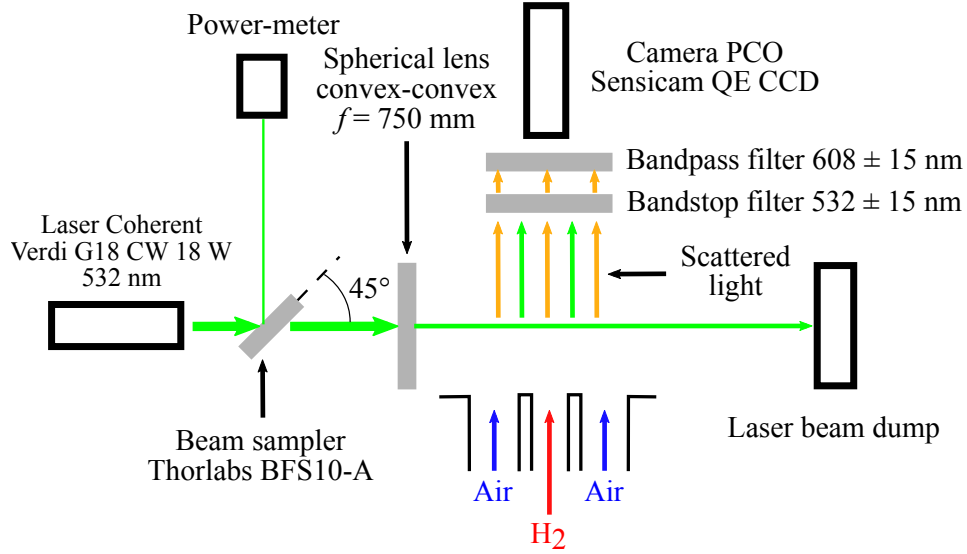


Figure 8: Schematic of the 1D1S Raman scattering optical system used in the experiments

## 4 Data Content, File Names and Formats

The data set includes temperatures, NOx concentrations, hydrogen molar fraction profiles in isothermal conditions and pressure drops in cold and hot flow conditions. It also includes the mean and rms velocity fields in the axial ( $x, z$ ) plane of the burner in cold and hot flow conditions.

Data are provided in the form of ASCII text files. The data set is organized in 2 directories, corresponding to each operating condition A and L. The file names are normalized to convey information about the type of flame (A, L), the type of data (velocity, temperature, molar fraction, NOx and pressure drop). For each flame, the data set is structured as follows:

Flame A → *Directory for the anchored flame A dataset*

- A\_NOx → *File .txt with NOx measurements*
- A\_OH\_star → *Directory with OH\* images*
- A\_PDdrop → *File .txt with the pressure drop values in each channel*
- A\_Raman → *File .txt with the molar fraction of hydrogen in cold flow conditions*
- A\_Temp → *Directory with the temperatures of the gas and the walls at the locations described section 3.5.*
  - \* T\_gas\_outlet
  - \* T\_gas\_z9
  - \* T\_gas\_z20
  - \* T\_wall\_chamber
  - \* T\_wall\_nozzle
- A\_Velocity\_PIV
  - \* A\_Cold → *Mean and RMS velocity fields in cold flow conditions*
  - \* A\_Reactive → *Mean and RMS velocity fields in reactive conditions*

Flame L → *Directory of the lifted flame dataset*

- L\_NOx
- L\_OH\_star
- L\_PDdrop
- L\_Raman

- L\_Temp
  - \* T\_gas\_outlet
  - \* T\_gas\_z9
  - \* T\_gas\_z20
  - \* T\_wall\_chamber
  - \* T\_wall\_nozzle
- L\_Velocity\_PIV
  - \* L\_Cold
  - \* L\_Reactive

Each text file comprises a header with:

- The name of the laboratory where the experiments were performed: Institut de Mécanique des Fluides de Toulouse (IMFT), France
- The version of the data file, referenced as HYLON\_TNF\_YEAR\_MONTH for data made available at year YEAR and month MONTH. Example: HYLON\_TNF\_2023\_01 for data taken in January (01) 2023.
- The flow operating conditions
- The geometrical configuration described in Fig. 2a, including the internal swirl level  $S_i$  and the external swirl level  $S_e$  [3]
- The type of data and the measurement technique used

#### 4.1 Flame\_NOx

NO, NO<sub>2</sub> and NOx corresponding to the sum of NO and NO<sub>2</sub> concentrations in ppm and O<sub>2</sub> concentration in % are reported in columns 1 to 4. Columns 5 to 7 report NO, NO<sub>2</sub> and NOx emissions for a reference with 15% of O<sub>2</sub>.

#### 4.2 Flame\_OH\_star

This directory contains 4 images. Burner.tif corresponds to the field of view without combustion. Mire.tif gives a grid pattern with a square of 1 mm size. X\_Mean\_n100.png is a line of sight image of the mean OH\* emission averaged over 100 instantaneous images. X\_Mean\_n100.abel.png is an Abel deconvoluted image of the OH\* distribution in the axial plane of the burner.

#### 4.3 Flame\_PDrop

The pressure drops in Pa in the air channel  $\Delta p_A$  and in the hydrogen channel  $\Delta p_H$  are reported in columns 1 and 2.

#### 4.4 Flame\_Raman

This text file has 5 columns. The first column gives the locations of the measurement along the  $x$ -axis in mm. The molar fractions  $X_{H_2}$  measured in cold flow conditions at this  $x$  location and 4 different heights  $z = 1, 2, 4$  and 6 mm are given in columns 2 to 5 respectively. These molar fractions were deduced from Raman scattering.

#### 4.5 Flame\_Temp

This directory comprises five sub-directories, two for the wall temperatures and three for the gas temperature at different locations. Temperature are given in Kelvin. The different files are:

- **T\_gas\_outlet** gives the temperature profile of the gas mixture along the  $x$ -axis at the fixed height  $z = 189$  mm, which corresponds to the combustion chamber exhaust nozzle outlet.

- **T\_gas\_z9** is the temperature of the gas in the Outer Recirculation Zone (ORZ), measured at  $x = 31.5$  mm and  $z = 20$  mm.
- **T\_gas\_z20** gives the temperature profile of the gases along the  $x$ -axis at the fixed height  $z = 20$  mm inside the combustion chamber.
- **T\_wall\_chamber** has 3 columns: the first column gives to the location of the measurements along the  $z$ -axis. The two others correspond to the temperature  $T_c$  and  $T_w$  at the external surface of one pillar (inox) and of one window (fused silica) respectively, as described Fig. 6(a).
- **T\_wall\_nozzle** has 2 columns: the first column corresponds to the temperature  $T_{s1}$  to  $T_{s9}$  which the location of the measurements is shown Fig. 6(b). The second column corresponds to the temperature in Kelvin.

## 4.6 Flame\_Velocity\_PIV

The velocity field has been investigated in cold and hot flow conditions with PIV measurements. The text files are structured as follows: Flame\_Condition (example A\_Cold for case A in cold flow conditions).

Each file has 6 columns: the first and second columns correspond to the location of the measurement along the  $x$ -axis and  $z$ -axis (mm). The 4 other columns correspond respectively to the mean radial velocity ( $U_r$ ), the mean axial velocity ( $V_z$ ), the RMS radial velocity ( $U_r_{rms}$ ) and RMS axial velocity ( $V_z_{rms}$ ) (m/s). Measurements are only valid:

- flame A in cold flow conditions :  $-25.1 \text{ mm} \leq x \leq 25.3 \text{ mm}$  and  $2.1 \text{ mm} \leq z \leq 41.8 \text{ mm}$
- flame A in hot flow conditions :  $-25.1 \text{ mm} \leq x \leq 25.3 \text{ mm}$  and  $2.1 \text{ mm} \leq z \leq 41.9 \text{ mm}$
- flame L in cold flow conditions :  $-25.1 \text{ mm} \leq x \leq 25.1 \text{ mm}$  and  $2.6 \text{ mm} \leq z \leq 41.9 \text{ mm}$
- flame L in hot flow conditions :  $-25.1 \text{ mm} \leq x \leq 25.3 \text{ mm}$  and  $2.5 \text{ mm} \leq z \leq 41.82 \text{ mm}$

## 5 Published work on HYLON burner

The impact of the internal swirl level  $S_i$  and the recess distance  $z_i$  on flame stabilization has been investigated in [3] for  $\text{CH}_4/\text{H}_2/\text{air}$  flames and in [4] for  $\text{H}_2/\text{air}$  flames.

The transition between lifted to anchored flame has been studied with a model described in [1, 4].

Some of the data presented in this document were compared to numerical flow simulations in [1]. In [1], hydrogen was replaced by air for cold flow measurements, the mass flow rate being imposed to conserve the momentum flux ratio  $J = (\rho_e u_e^2)/(\rho_i u_i^2)$ . In HYLON\_TNF\_2023\_04, cold flow measurements were made using hydrogen. As a result, comparisons between results from [1] and HYLON\_TNF\_2023\_04 for cold flow conditions need a special care.

## References

- [1] Andrea Aniello et al. “Experimental and numerical investigation of two flame stabilization regimes observed in a dual swirl H<sub>2</sub>-air coaxial injector”. In: *Combustion and Flame* 249 (2023), p. 112595. ISSN: 00102180. DOI: 10.1016/j.combustflame.2022.112595. URL: <https://linkinghub.elsevier.com/retrieve/pii/S0010218022006034>.
- [2] S Brohez, C Delvosalle, and G Marlair. “A two-thermocouples probe for radiation corrections of measured temperatures in compartment fires”. In: *Fire Safety Journal* 39 (2004), pp. 399–411. ISSN: 0379-7112. DOI: 10.1016/j.firesaf.2004.03.002. URL: <https://www.sciencedirect.com/science/article/pii/S037971120400027X>.
- [3] S. Marragou et al. “Stabilization regimes and pollutant emissions from a dual fuel CH<sub>4</sub>/H<sub>2</sub> and dual swirl low NO<sub>x</sub> burner”. In: *International Journal of Hydrogen Energy* 47 (44 2022), pp. 19275–19288. ISSN: 03603199. DOI: 10.1016/j.ijhydene.2022.04.033.
- [4] Sylvain Marragou et al. “Experimental analysis and theoretical lift-off criterion for H<sub>2</sub>/air flames stabilized on a dual swirl injector”. In: *Proceedings of the Combustion Institute* (2022). ISSN: 15407489. DOI: 10.1016/j.proci.2022.07.255. URL: <https://linkinghub.elsevier.com/retrieve/pii/S1540748922003248>.
- [5] D. V. Petrov. “Raman spectrum of methane in nitrogen, carbon dioxide, hydrogen, ethane, and propane environments”. In: *Spectrochimica Acta - Part A: Molecular and Biomolecular Spectroscopy* 191 (2018), pp. 573–578. ISSN: 13861425. DOI: 10.1016/j.saa.2017.10.058.